Journal of Power Sources 591 (2024) 233834

Contents lists available at ScienceDirect

Journal of Power Sources

journal homepage: www.elsevier.com/locate/jpowsour

Utilization of coal mine gas in solid oxide fuel cells: A performance evaluation

E.V. Tsipis [a,*], A.U. Sharafutdinov [a], D.V. Matveev [a], M.S. Dyakina [a], D.V. Zhigacheva [a], D.V. Yalovenko [a], A.P. Paduchev [b], S.I. Bredikhin [a], V.V. Kharton [a]

[a] Osipyan Institute of Solid State Physics RAS, 142432, Chernogolovka, Russia
[b] JSC "United Engine Corporation", Budennogo Ave. 16, Moscow, Russia

HIGHLIGHTS

- Coal mine gas can be directly utilized in SOFCs to produce electricity and heat.
- The minimum steam content for stable operation was estimated as 40.6 % at 1123 K.
- Complete internal CH_4 conversion and stable operation for 170 h were demonstrated.

ARTICLE INFO

Keywords:
SOFC stack
Waste gas utilization
Coal mine methane (CMM)
Steam reforming
Long-term operation
Carbon deposition

ABSTRACT

The possibility and regimes of coal mine gas utilization in solid oxide fuel cells (SOFCs) without external methane reforming were appraised using a short-stack of two membrane-electrode assemblies with the planar electrolyte-supported architecture. The stack fueled by model coal mine gas, namely 59 % CH_4 - 5 % CO_2 – 36 % N_2 mixture humidified at 343–363 K, demonstrated a stable operation during approximately 170 h at 1123 K when the fuel humidity was higher than 38 vol%. The performance decreased with increasing steam concentration and was lower than that obtained for hydrogen fuel at the same humidity levels. The maximum power density, 157 mW/cm^2 at the current density of 284 mA/cm^2, was observed for 38 % humidity close to the thermodynamic limit where carbon nanotube formation may start at the SOFC anode. Decreasing water vapor partial pressure resulted in a fast degradation, accompanied with increasing ohmic and polarization losses. Subsequent microscopic analysis confirmed that these effects are indeed associated with the carbon deposition. Beyond the coking domain, the current vs. voltage dependencies of the SOFC stack can be described by a simplified model assuming that the anode kinetics is essentially governed by the electrochemical oxidation of hydrogen.

1. Introduction

Despite the strengthening of environmental requirements, the global coal production continues growing every year [1–6]. In the course of coal mining, extraction of the mine gases containing CH_4 is critically necessary for the safety reasons. Moreover, abandoned mines release methane for a long period of time [7,8]. Recent analysis [3] showed that the emissions of coal mine methane (CMM) and abandoned mine methane (AMM) in 2010 were as high as 103×10^9 and 22×10^9 m^3, respectively. On the other hand, these gas mixtures present a source of methane that may be used for electrical and thermal energy generation. The utilization of mine methane is, however, still insufficient, especially in the case of the low-concentration drainage gas. This situation is associated, first of all, with explosivity, unstable composition and inconstant emission rates [7,8]. The gases from coal deposits comprise CH_4 and other products of the coal metamorphism, namely heavy homologues of methane, hydrogen, hydrogen sulfide as well as the gases of atmospheric air origin (CO_2, N_2 and inert gases), which penetrate the coal seam due to gas weathering [9]. For the high-temperature utilization technologies, the particulate removal, deoxygenation and sulfur removal are often necessary. The ventilation air methane (VAM) containing typically $\leq$1 % of CH_4 is the largest source of methane for most mines [6–8]. However, utilization of such diluted gas mixtures is problematic, mainly due to their low calorific value. Even in the case of

* Corresponding author.
E-mail address: tsipis@issp.ac.ru (E.V. Tsipis).

https://doi.org/10.1016/j.jpowsour.2023.233834
Received 8 September 2023; Received in revised form 25 October 2023; Accepted 6 November 2023
Available online 11 November 2023
0378-7753/

higher-concentration CMM, large variations in methane and oxygen concentrations may cause serious problems for its use in the conventional engines, such as reciprocating internal combustion engines and gas turbines [9,10]. Significant efforts are hence centered on the development of alternative approaches [4–8,10–13].

The technologies based on solid oxide fuel cells (SOFCs) adapted for the use of coal mine gas are considered efficient to produce electrical power and heat [10,12,13]. Important advantages of SOFCs include relatively low requirements for the fuel purity and an ability to operate using various types of gaseous fuels, including light hydrocarbons. There exists, however, a lack of systematic experimental data on SOFC operation using the coal mine gases. Preliminary experiments [14] demonstrated an operation of one SOFC stack made of the conventional electrode and electrolyte materials, employing a model CH_4-containing gas mixture without external reforming. For 47 % CH_4 - 53 % CO_2 fuel humidified at 338 K, the maximum power density was 0.18 W/cm^2 at 1123 K. The methane content in the exhaust gas flux was 0.01 vol%, indicating a sufficiently high utilization degree. A fuel consumption of 6.3 dm^3/min in terms of dry gas was estimated for 1 kW system [14].

One important problem associated with the use of hydrocarbon-containing fuels in SOFCs, is related to carbon deposition on the conventional Ni-based anodes and resultant degradation in the SOFC performance (e.g. Refs. [15,16]). This factor makes it necessary to determine minimum steam concentration in the fuel, required to exclude hydrocarbon pyrolysis (cracking) and Boudouard reaction (CO disproportionation) in each particular case.

Continuing previous research [14,15], the present work is focused on the appraisal of coal mine gas utilization in the planar electrolyte-supported SOFCs operating at 1123 K, with a special attention to relationships between the fuel gas humidity and fuel cell stack performance. Although the anode-supported SOFC architecture makes it possible to substantially decrease the cell resistance and operation temperature, the internal conversion of methane and minimization of coking risks require relatively high operating temperatures, above 1100 K. Also, the supporting electrolyte membranes possess a higher mechanical strength with respect to those used for the anode-supported cells, which may be critical in case of massive carbon deposition at the anode/electrolyte interface. The electrochemical tests of a SOFC stack fueled by model mine gas were carried out, including impedance spectroscopy, analysis of the current-voltage (I–V) dependencies and power density, and life tests. One-dimensional model of a SOFC stack operating using coal mine gas was proposed and validated. The gas mixture compositions dangerous from the carbon deposition point of view were determined according to the C–H – O phase diagram. The main aims were to assess the SOFC operation regimes feasible for the mine gas utilization, to evaluate stability of the stack components in the conditions of direct methane oxidation, and to collect new experimental data necessary for the development of pilot SOFC-based systems.

2. Experimental section

In order to study the operational features of SOFCs using a model coal mine gas, a short-stack with two planar membrane-electrode assemblies (MEAs) was produced. Fig. 1A illustrates the microstructure of one fractured MEA. The solid electrolyte is a three-layer gas-tight plate (10 × 10 cm^2 in size) consisting of one 90 μm thick internal layer of 10 mol.% Sc_2O_3 and 1 mol.% Y_2O_3 co-stabilized ZrO_2 (10Sc1YSZ) and two 30 μm thick external layers of 6 mol.% Sc_2O_3-stabilized ZrO_2 (6ScSZ). The electrode layers with geometric area of 9 × 9 cm^2 were applied by screen printing using an EKRA E2 instrument (EKRA Innovative Technologien, Germany). The electrode pastes were prepared by mixing of ball-milled oxide powders with an organic binder. After deposition, the electrode layers were dried and finally co-sintered in air at 1523 K. The porous cathodes comprised one protective interlayer of $Ce_{0.9}Gd_{0.1}O_{1.95}$ (GDC10), composite $(Pr_{0.6}Sr_{0.4})_{0.97}MnO_{3-\delta}$ (PSM) - GDC10 (60–40 wt%) functional layer and $(La_{0.6}Sr_{0.4})_{0.97}MnO_{3-\delta}$ (LSM) current-collecting

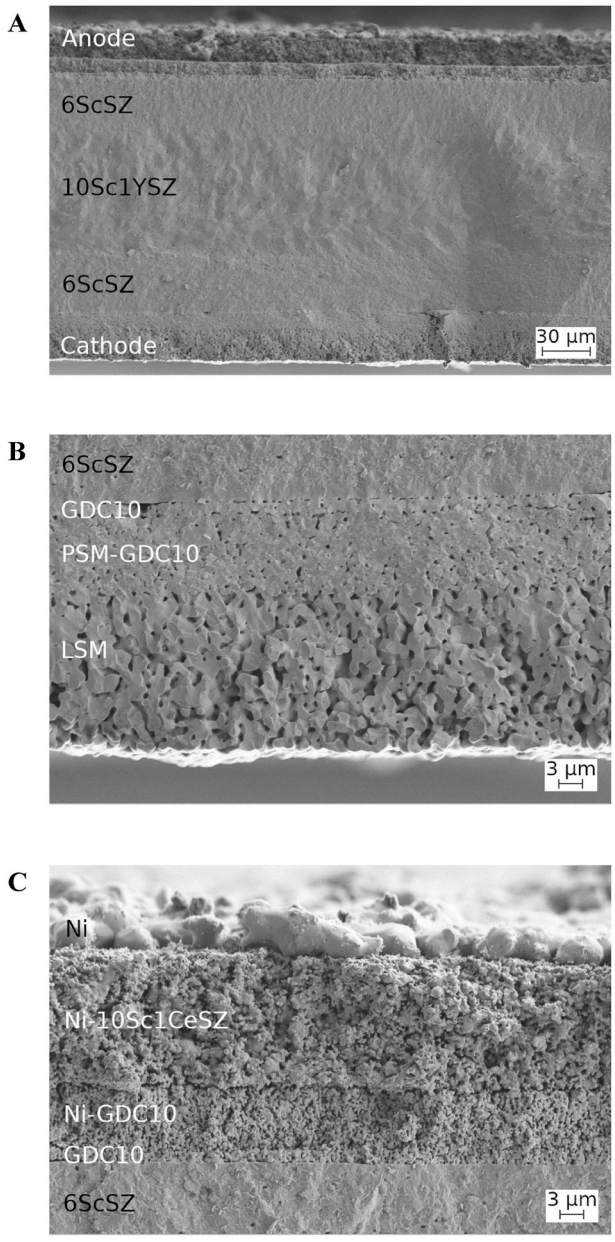

Fig. 1. SEM images of a fractured MEA after testing (A), porous cathode (B) and of anode (C).

layer (Fig. 1B and 2A). Single-phase PSM and LSM perovskites (Fig. 3) were synthesized via the glycine-nitrate process. All other powders were commercially available. Phase purity of all components was confirmed by the X-ray diffraction (XRD) analysis using a Rigaku SmartLab SE instrument (CuK_α radiation). The anode consisted of successive GDC10, NiO - GDC10 composite (50 - 50 wt%), NiO–10Sc1CeSZ composite (60–40 wt%) and NiO layers (Fig. 1C and 2A). The current collectors were made of Ni-coated Crofer 22H stainless steel (Fig. 2A). The contact layers of LSM and NiO pastes were deposited on the current collectors and on the nickel mesh covering the anode, respectively. A commercially available high-temperature glass-ceramic sealant (Kerafol, Germany) was used to separate the anode and cathode chambers and to hermetically seal the assembly.

The produced model short-stack was installed in an Evaluator C1000-HT (Horiba FuelCon, Germany) test setup under the mechanical load of 0.33 kg/cm^2, as illustrated in Fig. 2B. After sealing at 1213 K, the measurements were performed at 1123 K using a Reference 3000

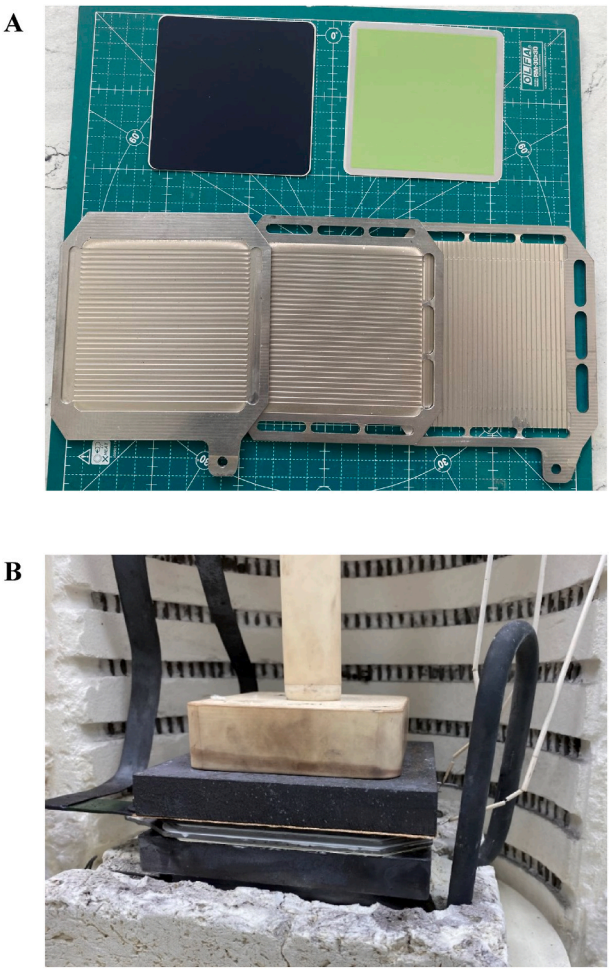

Fig. 2. Photos of the SOFC stack components (A) and short-stack placed in the furnace (B).

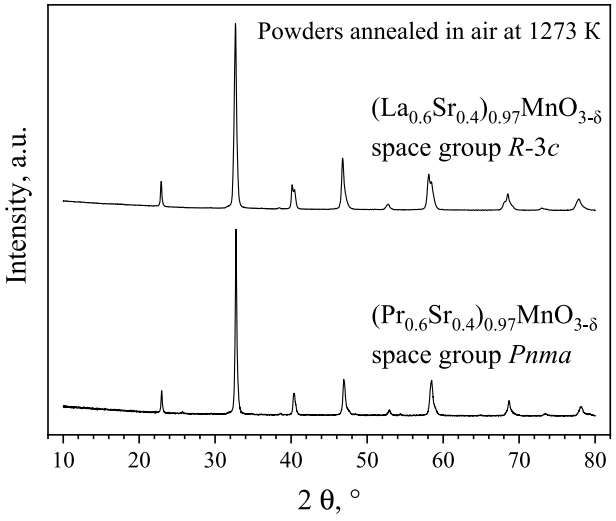

Fig. 3. X-ray diffraction patterns of as-synthesized $(La_{0.6}Sr_{0.4})_{0.97}MnO_{3-\delta}$ и $(Pr_{0.6}Sr_{0.4})_{0.97}MnO_{3-\delta}$ powders.

potentiostat-galvanostat (Gamry Instuments, USA) equipped with a Reference 30 k booster. The gas flow rates were settled by the mass-flow controllers (Bronkhorst Instruments, Germany). Atmospheric air (3000 ml/min) was supplied onto the cathodes; H_2 (600 ml/min) or the mixture of 59 % CH_4 - 5 % CO_2 – 36 % N_2 (295 ml/min) humidified at various temperatures was supplied into the anodic chamber. The scanning electron microscopy coupled with energy dispersive spectroscopy (SEM/EDS) employing a Supra 50VP microscope (CarlZeiss, Germany) was used for the microstructural and elemental analysis after the stack tests. Modelling of the experimental data was performed using COMSOL Multiphysics software.

3. Results and discussion

3.1. Performance and stability of the SOFC stack fueled by hydrogen

The stack performance at 1123 K was evaluated at the fuel humidifier temperatures of 343, 348, 353, 358, and 363 K, which correspond to the humidity of 31, 38, 47, 57 and 69 %, respectively. In order to test stability of the assembly when using pure hydrogen as a fuel, the model SOFC stack was kept for at least 6 h at a constant direct current of 15 A (185 mA/cm^2) for the humidities of 31–57 % and 12 A (148 mA/cm^2) for 69 % humidity after each I–V and impedance measurement. Fig. 4A shows the time dependencies of voltage at a constant current density for various steam concentrations in the influent fuel mixture. After switching 5 % H_2 - Ar gas mixture to 31%-humidified H_2, the power density exhibited a continuous growth during the next 15–20 h. For the first 13 h, its value increased from 130 to 145 mW/cm^2 at an operating voltage of 1.4 V (0.7 V per MEA), and from 167 to 183 mW/cm^2 at a current density of 333 mA/cm^2, Fig. 5A. On further testing, the voltage remained essentially constant (Fig. 4A).

Fig. 6A displays the current dependencies of voltage and power for different humidity levels (31–69 %) at the inlet. The power densities vary from 106 to 146 mW/cm^2 at an operating voltage of 0.7 V per MEA, decreasing when the steam content in the fuel increases (Fig. 6A). This behavior is in agreement with the literature data [17] and originates,

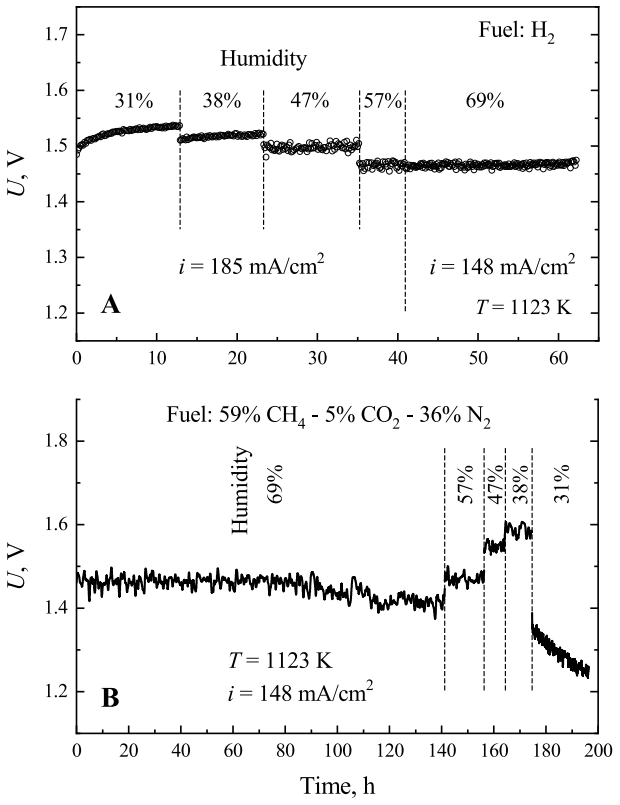

Fig. 4. Time dependencies of the voltage for the two-MEA SOFC stack operating on pure hydrogen (A) and model coal mine gas (B) with different steam concentrations at 1123 K and current loads of 148–185 mA/cm^2.

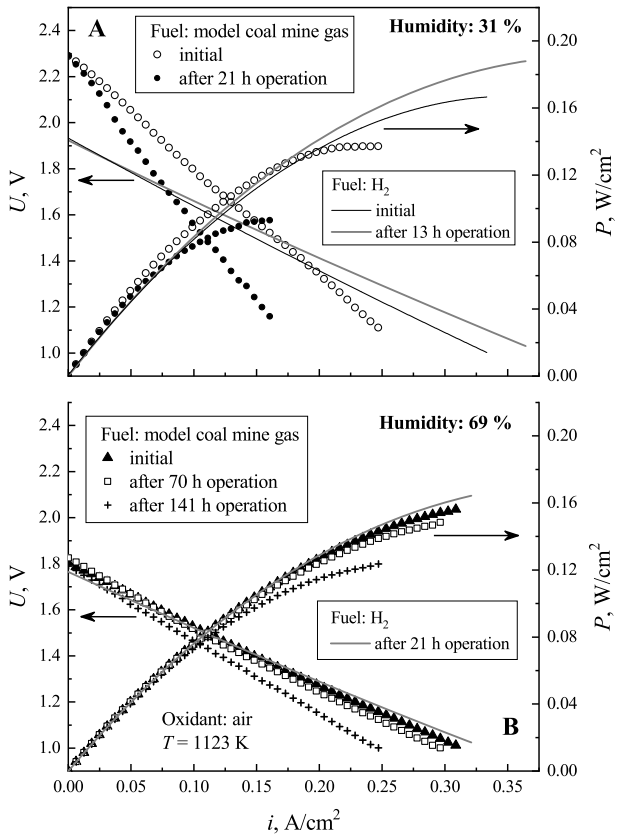

Fig. 5. Comparison of the current-voltage curves and power densities of the SOFC short-stack operating at 1123 K using H_2 and model coal mine gas humidified at 343 K (A) and 363 K (B).

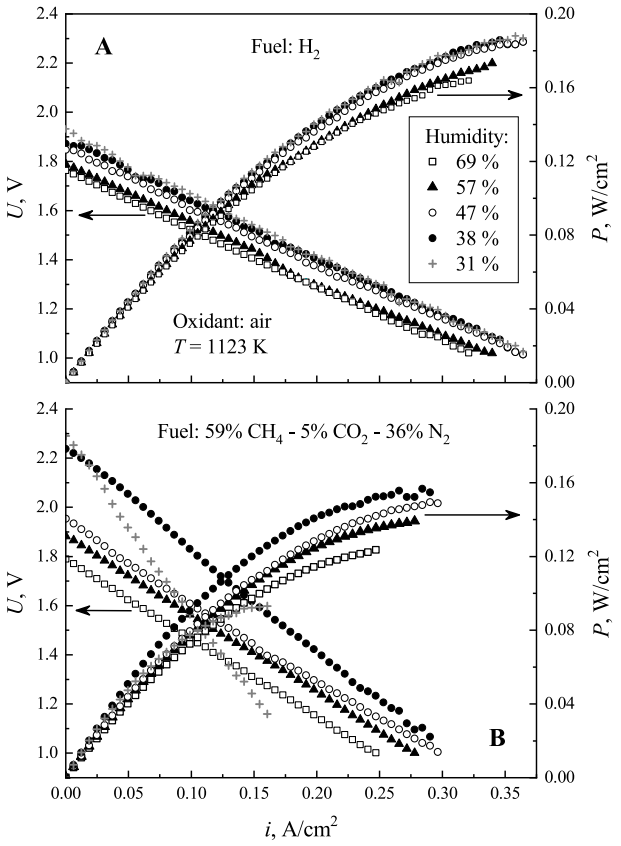

Fig. 6. Current-voltage dependencies and power densities of the SOFC stack operating at 1123 K using H_2 (A) and model coal mine gas (B), humidified at 343–363 K.

first of all, from the dependence of the open-circuit voltage (OCV) on H_2: H_2O ratio in the fuel. The anode exchange currents and overpotentials are also dependent on the hydrogen/steam ratio (e.g., see Refs. [15,17] and references therein). Moreover, excessively high humidity may induce local oxidation at the anode and current-collector surfaces. The peak power of 30.3 W (187 mW/cm^2) was observed for 38-47 %-humidified hydrogen at 1123 K and current of 29.5 A (364 mA/cm^2). Testing in hydrogen atmosphere demonstrated, hence, gas-tightness of the model stack and its suitability for further studies in the methane-containing fuel. The data collected under hydrogen/air gradient were used as input for modelling of the SOFC operation using coal mine gas.

3.2. Testing of the SOFC stack fueled by coal mine gas

At the next stage, the fuel was changed and the model coal mine gas (59 % CH_4 - 5 % CO_2 – 36 % N_2) was supplied into the stack. As expected, the SOFC performance obtained for the mine gas is generally worse than that for hydrogen fuel (Fig. 6). The use of 69 %-humidified mine gas as a fuel leads to complete internal conversion of methane. In the methane steam reforming reaction, three molecules of hydrogen and one molecule of carbon monoxide are formed; all these components are then oxidized in SOFCs. The differences in the open-circuit voltage (OCV) observed when using pure hydrogen and converted mine gas as fuels (Figs. 5 and 6), result from the presence of CO in the latter case. The cell voltage was stable during the first 70 h of operation at the constant current load of 148 mA/cm^2, and started to decrease on further exposure (Fig. 4B). After 113 h of operation, the voltage stabilized and became approximately 3 % lower compared to the initial level. Fig. 5B compares the current dependencies of voltage and power obtained at the initial step, after 70 h, and after 141 h of testing at the DC density of 148 mA/cm^2 in 69 %-humidified mine gas. The decrease in SOFC performance, especially pronounced at high current densities, may be indicative of irreversible changes at the anode/interconnector interface associated with local oxidation of metallic current collectors and/or nickel at the inlet zone due to excessively high fuel humidity.

At the fuel humidities of 38–57 %, a stable performance was obtained (Fig. 4B). The corresponding current-voltage characteristics are shown in Fig. 6(B). The maximum power density of 157 mW/cm^2 was achieved for 38 %-humidified coal mine gas at 1123 K and current density of 284 mA/cm^2. After decreasing humidity down to 31 %, a rapid degradation in the SOFC performance and an increase in the ohmic and polarization resistances were observed. These changes are associated with carbon deposition at the anode surface, confirmed by the results of post-operational SEM/EDS analysis (Fig. 7). Notice that, after the SOFC operation, no microstructural changes of the electrodes were observed and the percolation of nickel was retained (Fig. 1). However, a significant amount of carbon was deposited at the anode surface. The critical level of water vapor concentration in the coal mine gas should be, therefore, close to 38 vol%. This level corresponds to minimum required to enter the methane steam reforming mode and to exclude methane pyrolysis. Such a conclusion is consistent with the C–H – O phase diagram, discussed below, and were further verified by modelling of the current-voltage dependencies of the SOFC short-stack operating on coal mine gas.

3.3. Modelling of the current vs. voltage dependencies

The SOFC model used in this work was based on the following starting assumptions. As the SOFC short-stack consisted of two MEAs sandwiched between 2 cm thick steel plates, the temperature distribution can be considered uniform (local temperature deviations lower than

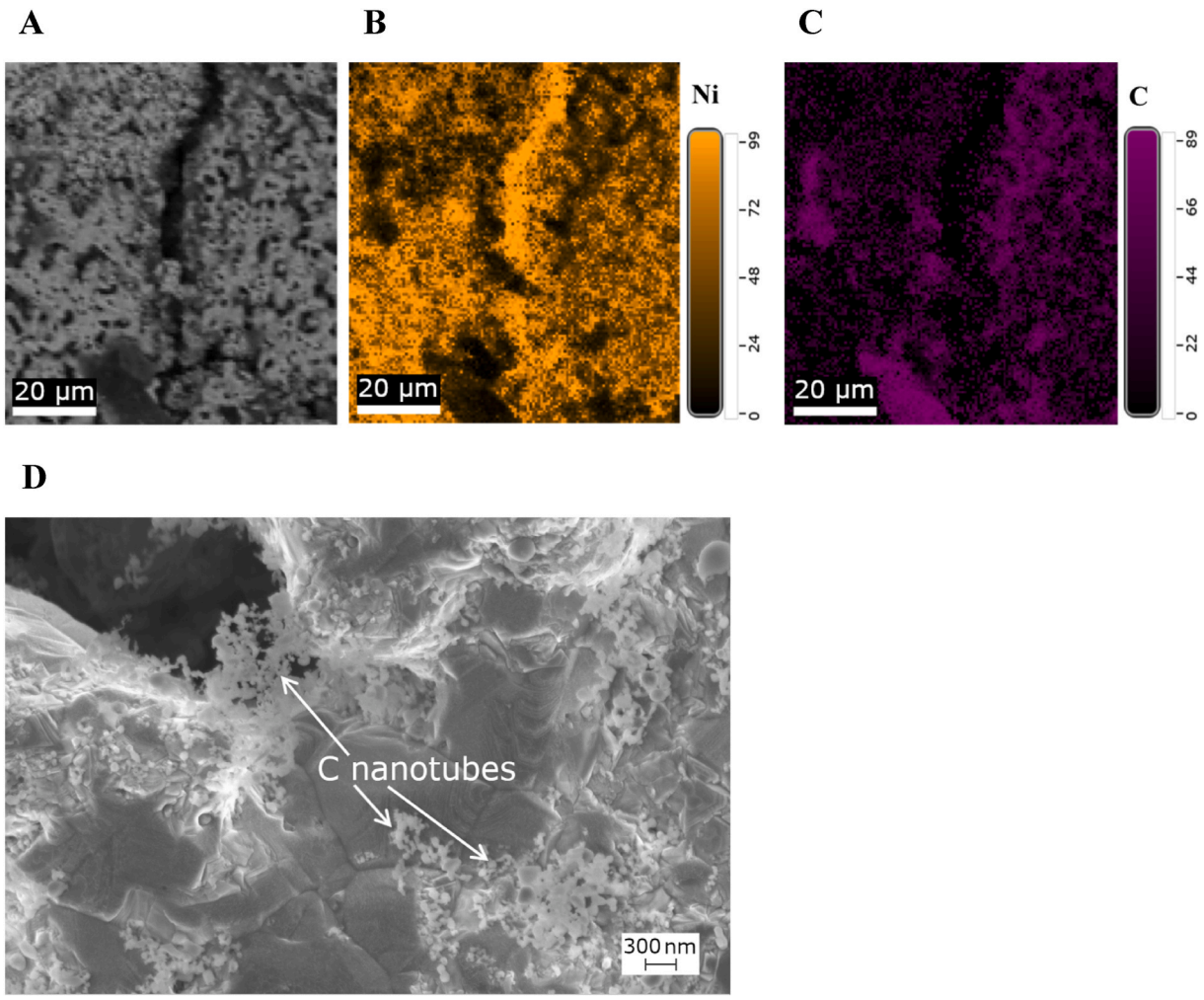

Fig. 7. SEM image (A) and corresponding mapping of nickel (B) and carbon (C) distribution for the anode surface after testing in coal mine gas, and SEM image of the carbon deposits (D).

1 K). Taking into account the high electrical conductivity of the stainless steel and geometry of the planar gas-distribution channels, the electrodes may be assumed equipotential, whilst the fuel supply along MEAs is homogeneous. In this case, one-dimensional approach should be applicable, where the presence of air crossflow can be accounted implicitly by reducing the Nernst potential. The binary diffusion coefficients were approximated by extrapolation of the tabulated data according to the Chapman-Enskog theory [18]. Since excess air was supplied onto the cathodes, the correction for decreasing oxygen concentration in this flow should be small. The depth of the gas channels, 400 μm for the fuel and 800 μm for the air chambers, is small enough to consider the gas flows as laminar. Moreover, as the diffusion coefficients of the gaseous phase components are sufficiently high, the fuel composition in the direction perpendicular to its flow was assumed homogeneous, with the compositional deviations lower than 1 %. At the same time, diffusion along the fuel path can be neglected with respect to the convective flow rate; the diffusion flow is lower than 0.5 % of the convective one. In light of the above assumptions, the mass conservation principle is sufficient to determine the gas mixture composition along the fuel path:

$$A_{ch}\frac{\partial}{\partial t}(C_{tot}x_i)+\frac{\partial}{\partial l}(N_{tot}X_i)=S_i \tag{1}$$

where A_{ch} (m^2) is the total cross-section area of the gas channels, t (s) is the time, C_{tot} (mol/m^3) is the total molar concentration, l is the coordinate along fuel path, N_{tot} (mol/s) is the total fuel flow, X_i is the molar fraction of i-th component, and S_i (mol × s^{-1} × m^{-1}) is the generation rate of the i-th component per unit length. For the steady-state conditions, Eq. (1) can be simplified:

$$\frac{\partial}{\partial l}(N_{tot}X_i)=S_i \tag{2}$$

The calculation of S_i should take into account the reactions of steam reforming of methane (SMR), water-gas shift (WGS) and hydrogen oxidation (HO):

$$CH_4+H_2O\longleftrightarrow 3H_2+CO\ \frac{P_{CO}P_{H2}^3}{P_{H2O}P_{CH4}}=K_{\mathrm{SMR}} \tag{3}$$

$$H_2O+CO\longleftrightarrow H_2+CO_2\ \frac{P_{CO2}P_{H2}}{P_{CO}P_{H2O}}=K_{\mathrm{WGS}} \tag{4}$$

$$H_2+\frac{1}{2}O_2\leftrightarrow H_2O\ \frac{P_{H2O}}{P_{H2}P_{O2}^{1/2}}=K_{\mathrm{HO}} \tag{5}$$

where K_{SMR}, K_{WGS} and K_{HO} are the corresponding equilibrium constants provided in the NIST thermochemical data [19], and P_i (bar) is the i-th component partial pressure. Note that the CO oxidation reaction was not taken into account, since its rate is several times lower than the rate of hydrogen oxidation [20]; CO is therefore consumed in the reaction expressed by Eq. (4). Then S_i is expressed as:

$$S_i = \frac{A_{ch}}{h_{ch}}\left(n_i^{SMR}R_{SMR} + n_i^{WGS}R_{WGS} + n_i^{HO}R_{HO}\right) \quad (6)$$

where R_x (mol × m^{-3} × s^{-1}) and n_i^x are the rates and stoichiometric vectors of the corresponding reactions (Eqs. (3)–(5)), respectively, and h_{ch} is the depth of the fuel channels. The SMR rate is expressed as:

$$R_{SMR} = k_1\left(\frac{k_2 P_{CH_4}P_{H_2O}\left[1 - \frac{P_{CO}P_{H_2}^3}{K_{SMR}P_{CH_4}P_{H_2O}}\right]}{P_{H_2O} + b_2P_{H_2}^2 + b_3P_{H_2}^3}\right) \quad (7)$$

where

$$k_2 = \frac{3\times10^{13}}{T^3}e^{-\frac{141287}{RT}}, b_2 = \frac{8,12\times10^3}{T^3}e^{\frac{81789}{RT}} \text{and} b_3 = \frac{1,82\times10^7}{T^{6,5}}e^{\frac{195673}{RT}}$$

R is the universal gas constant, T (K) is the temperature, the coefficient k_1 (mol × m^{-2} × s^{-1}) depends on the specific surface area and morphology of Ni catalyst and was hence used as a fitting parameter; k_2, b_2 and b_3 are the coefficients depending on the rate constants of elementary reaction steps [21]. The water-gas shift reaction rate and its constant can be expressed as

$$R_{WGS} = k_3P_{tot}X_{CO}\left(1 - \frac{X_{CO2}X_{H2}}{K_{\mathrm{WGS}}X_{CO}X_{H2O}}\right) \text{and} K_{\mathrm{WGS}} = e^{\frac{4276}{T} - 3.961} \quad (8)$$

where P_{tot} is the total pressure. Since the kinetics of reaction expressed by Eq. (4) is very fast, its deviation from equilibrium should be negligibly small. Therefore, P_{tot} was assumed constant along the path; the value of $k_3 = 3\times10^{-6}$ mol × m^{-2} × s^{-1} × bar^{-1} was chosen arbitrarily, large enough to ensure that the WGS reaction is close to equilibrium [22]. For the hydrogen oxidation rate

$$R_{HO} = \frac{i}{2F} \quad (9)$$

where F is the Faraday constant and i (A/cm^2) is the local current density. The latter quantity is directly related to the local sum of anodic and cathodic overpotentials $\eta = E_{eq} - U$, where E_{eq} and U are the Nernst and cell voltages, respectively. The empirical overpotential-current relationship was extracted from the experimental results obtained for humidified hydrogen fuel (Fig. 6A): $i(\eta) = 1.06\eta - 0.151\tanh\frac{\eta}{0.3754}$.

The Nernst voltage corrected for the oxygen losses from flowing air can be determined by the first order perturbation equation:

$$E_{eq} = E_{eq}^0 - \frac{RT}{8F}\frac{i}{i_{O2}X_{O2}} \quad (10)$$

where

$$E_{eq}^0 = E_0 + \frac{RT}{2F}\ln\frac{X_{H2}}{X_{H2O}}X_{O2}^{1/2} + \frac{RT}{2F}\ln\frac{P_{tot}}{P_{ref}}, i_{O2} = \frac{4Ff_{air}X_{O2}}{A_{MEA}}$$

and

$$E_0 = 1.26481 - \frac{3.95}{T} - 0.00012125T - 2.542\times10^{-8}T^2 + 1.006\times10^{-11}T^3 - 1.381\times10^{-15}T^4 - - 0.000018071T\ln T$$

In these formulae, i_{O2} is the theoretical faradaic current expected in the case of 100 % consumption of oxygen supplied into the cathode chamber, $P_{ref} = 1$ bar is the reference pressure, f_{air} is the air flow, $f_{air}x_{O2}$ is the molar oxygen flux, A_{MEA} is the electrode area for each MEA, and E_0 is the partial pressure-independent contribution to the Nernst potential approximated from NIST data in the temperature range of 1000–1700 K [19].

Equations 2–10 were used for nonlinear regression analysis of the experimental current-voltage curves obtained for the SOFC short-stack fueled by the model coal mine gas. The coefficient K_1 = 29.6 mol × m^{-2} × s^{-1} was determined by minimizing the root-mean-square deviation from the experimental I–V curves simultaneously at three humidity levels (69 %, 57 %, and 47 %). The model fits well to the experimental data up to the onset of carbon deposition at the anode, Fig. 8A. The latter process occurs already at 38 vol% humidity, which was not obvious from the data presented in Fig. 4B and 6B. Increasing current load and, thus, oxygen flux should progressively suppress coking. Consequently, the model and experimental data become closer to one another when the current increases (Fig. 8A); for 38 % humidity at the current densities corresponding to peak power values, these nearly coincide. The same reason is responsible for the fact that no performance degradation was observed at the current density of 148 mA/cm^2 for 10 h (Fig. 4B). However, when the dynamic equilibrium is settled at the anode under open-circuit conditions, the thermodynamic data show that solid carbon should form at 38 % humidity and 1123 K.

3.4. Carbon formation under equilibrium conditions

The minimum humidity levels acceptable for the coal mine gas utilization in SOFCs, can be determined by analyzing the carbon formation limits under thermodynamic equilibrium conditions. For these calculations, the Boudouard reaction:

$$2\mathrm{CO} \longleftrightarrow \mathrm{C} + \mathrm{CO_2}\ \frac{a_C P_{CO2}}{P_{CO}^2} = K_{\mathrm{BD}} \quad (11)$$

where a_C is the chemical activity of carbon, should be taken into account in combination with WGS and SMR reactions (Eqs. (3) and (4)). The equilibrium gas mixture composition is only a function of total pressure, temperature, and the content of hydrogen, oxygen and carbon:

$$P_{CH4} + P_{CO} + P_{CO2} = P_{tot}\frac{X_C}{X_{tot}} \quad (12)$$

$$P_{H2} + P_{H2O} + 2P_{CH4} = P_{tot}\frac{X_{H2}}{X_{tot}} \quad (13)$$

$$P_{CO} + 2P_{CO2} + P_{H2O} = P_{tot}\frac{X_O}{X_{tot}} \quad (14)$$

$$X_{H2} + X_O + X_C = 1 \quad (15)$$

$$X_{tot} = \left(\frac{P_{H2} + 2P_{CO} + 2P_{H2O} + 3P_{CO2} + 3P_{CH4}}{P_{total}}\right)^{-1} \quad (16)$$

where X_O, X_C, X_H are the molar fractions of O, C and H atoms in the gas mixture, respectively; $X_{tot} = \frac{N_{H2}+N_{CO}+N_{H2O}+N_{CO2}+N_{CH4}}{N_O+N_C+N_H}$ is the ratio of the total number of molecules to the number of O, C and H atoms. The influent gas compositions with various humidity levels are shown in Fig. 8B in the C–H – O coordinates according to Eqs. (3), (4), (11)–(16), taking into account the presence of N_2 in the model coal mine gas.

One should also mention that solid carbon may be deposited in various forms (graphite, multi- and single-walled nanotubes, or soot) having different values of the Gibbs formation energy. At temperatures

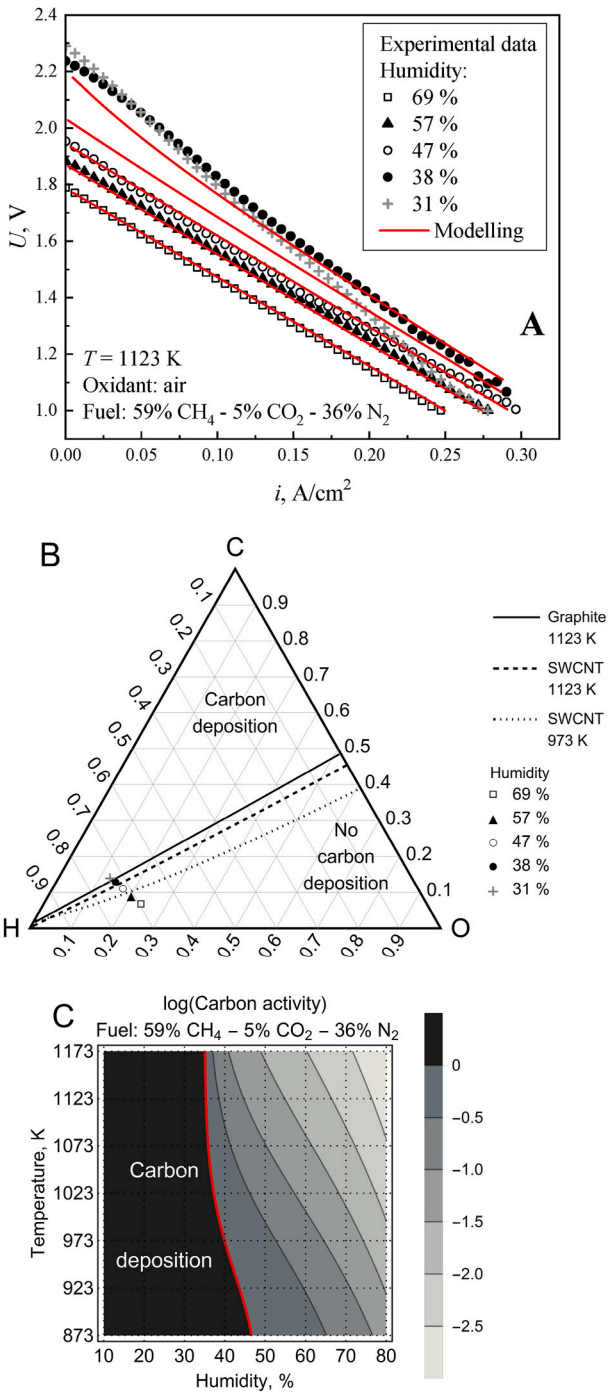

Fig. 8. Experimental (points) and calculated (lines) current-voltage curves for the SOFC short-stack operating on humidified coal mine gas (A), C–H – O ternary diagram showing the experimental influent gas compositions (points) and iso-activity lines at $a_C = 1$ for different forms of carbon at atmospheric total pressure (B) and carbon activity (decimal logarithm) as a function of temperature and fuel humidity (C). The thick red line in (C) corresponds to the carbon iso-activity line at $a_C = 1$ for graphite. (For interpretation of the references to colour in this figure legend, the reader is referred to the Web version of this article.)

above 873 K, formation of the single-walled carbon nanotubes (SWCNT) is energetically favorable [23]. Comparison between the carbon deposition boundaries [23] at 1123 K and influent fuel compositions used in this work (Fig. 8B) suggests that carbon should deposit at the anode surface in the form of nanotubes, but not as graphite. The formation of carbon nanotubes was, indeed, clearly visible in the SEM micrographs (Fig. 7D).

Finally, consideration of the SWCNT deposition limit at 973 K [23] makes it possible to assess the safe regime of SOFC stack operation using coal mine gas. The short-stack tested in this work is small enough and can hence be considered as nearly isothermal. For larger stacks, the temperature gradients should unavoidably increase. Such gradients, either along the MEAs or across the layers, may lead to thermal-induced cell fractures [22,24,25]. Taking into account the thermal expansion coefficient of the solid electrolyte ceramics, and assuming a maximum safe stress-induced linear strain of 0.1 %, the maximum allowable temperature gradient was estimated as 100 K per 10 cm length of MEA [24]. Modelling of temperature variations along and across the cells showed, however, that the gradients may exceed this limit, depending on the gas flow arrangement in the stack [22,25]. Therefore, possible coking at 973–1023 K should also be taken into account (Fig. 8B). The calculated critical values of water vapor content in the influent 59 % CH_4 - 5 % CO_2 – 36 % N_2 fuel are 51.6 and 40.6 vol% at 973 and 1123 K, respectively.

4. Conclusions

The SOFC short-stack of two electrolyte-supported planar MEAs was produced and tested using model coal mine gas, 59 % CH_4 - 5 % CO_2 – 36 % N_2, as a fuel. The MEAs comprised 150 μm thick three-layer zirconia solid electrolyte membranes, manganite-based cathodes and Ni-containing cermet anodes. As expected, the SOFC performance obtained for the humidified mine gas is lower than that for pure hydrogen at the same humidity levels and decreases with increasing steam concentration. At high fuel humidities, complete conversion of methane and a stable operation during approximately 170 h were observed. The maximum power density, 157 mW/cm^2, was achieved for 38 %-humidified fuel at 1123 K and current density of 284 mA/cm^2. Decreasing humidity down to 31 % resulted in a rapid degradation in the SOFC performance, accompanied with an increase in both ohmic and polarization losses extracted from the impedance spectra. This degradation originates from carbon deposition at the anode surface, as confirmed by SEM/EDS analyses and thermodynamic calculations. Comparison of the experimental results and equilibrium boundaries of carbon formation in various forms showed that carbon nanotube growth may start at the anode when the fuel humidity is too low. The experimental current-voltage dependencies coincide with theoretical ones derived using a 1D SOFC model up to the onset of anode coking. The estimated minimum level of the coal mine gas humidity necessary for stable long-term operation of SOFCs, is approximately 40.6 % at 1123 K.

Author statement

E.V. Tsipis: Conceptualization, Investigation, Visualization, Writing – original draft, A.U. Sharafutdinov: Methodology, Formal Analysis, Visualization, Writing – original draft, D.V. Matveev: Methodology, Investigation, Data curation, Writing – original draft, M.S. Dyakina: Investigation, D.V. Zhigacheva: Investigation, D.V. Yalovenko: Investigation, A.P. Paduchev: Conceptualization, Validation, S.I. Bredikhin: Conceptualization, Supervision, Validation, V.V. Kharton: Conceptualization, Supervision, Validation, Writing – review & editing.

Declaration of competing interest

The authors declare that they have no known competing financial interests or personal relationships that could have appeared to influence the work reported in this paper.

Data availability

Data will be made available on request.

Acknowledgments

Financial support from the Russian Science Foundation (grant 20-19-00478) is gratefully acknowledged.

References

[1] W. Wang, H. Li, Y. Liu, M. Liu, H. Wang, W. Li, Addressing the gas emission problem of the world's largest coal producer and consumer: lessons from the Sihe Coalfield, China, Energy Rep. 6 (2020) 3264–3277, https://doi.org/10.1016/j.egyr.2020.11.199.

[2] O. Tailakov, D. Zastrelov, V. Tailakov, M. Makeev, P. Soot, Utilization prospects for coal mine methane (CMM) in Kuzbass, E3S Web Conf. 15 (2017), 02002, https://doi.org/10.1051/e3sconf/20171502002.

[3] N. Kholod, M. Evans, R.C. Pilcher, V. Roshchanka, F. Ruiz, M. Coté, R. Collings, Global methane emissions from coal mining to continue growing even with declining coal production, J. Clean. Prod. 256 (2020), 120489, https://doi.org/10.1016/j.jclepro.2020.120489.

[4] R.D. Tate, Bigger than oil or gas? Sizing up coal mine methane, in: Global Energy Monitor Report, 2022. https://globalenergymonitor.org/wp-content/uploads/2022/03/GEM_CCM2022_r4.pdf. (Accessed 12 June 2023).

[5] Global Methane Initiative. https://www.globalmethane.org. (Accessed 12 June 2023).

[6] Coalbed Methane Outreach Program (CMOP), US Environmental Protection Agency (EPA). https://www.epa.gov/cmop (assessed 12 June 2023).

[7] C.Ö. Karacan, F.A. Ruiz, M. Cotè, S. Phipps, Coal mine methane: a review of capture and utilization practices with benefits to mining safety and to greenhouse gas reduction, Int. J. Coal Geol. 86 (2011) 121–156, https://doi.org/10.1016/j.coal.2011.02.009.

[8] S. Su, A. Beath, H. Guo, C. Mallett, An assessment of mine methane mitigation and utilisation technologies, Prog. Energy Combust. Sci. 31 (2005) 123–170, https://doi.org/10.1016/j.pecs.2004.11.001.

[9] R.Z. Tumashev, N.L. Shegolev, D.M. Kulakov, Coal mine methane utilization in gas turbine units for electricity and heat production, Safety in the technosphere 5 (2015) 41–48, in Russian.

[10] B. Groß, L. Blum, L.G.J. de Haart, A. Dengel, Development of a solid oxide fuel cell for the utilization of coal mine gas, J. Power Sources 196 (2011) 5309–5316.

[11] Comprehensive scientific and technical program of the full innovation cycle "Clean Coal - Green Kuzbass". https://minobrnauki.gov.ru/press-center/news/main/25560/(assessed 12 June 2023). in Russian.

[12] X. Wang, F. Zhou, Y. Ling, Y. Xiao, B. Ma, X. Ma, S. Yu, H. Liu, K. Wei, J. Kang, Overview and outlook on utilization technologies of low-concentration coal mine methane, Energy Fuel. 35 (2021) 15398–15423, https://doi.org/10.1021/acs.energyfuels.1c02312.

[13] H. Chen, Y. Wu, G. Yang, J. Shi, W. Zhou, J. Bai, Z. Shao, Direct power generation from low concentration coal-bed gas by a catalyst-modified Solid Oxide Fuel Cell, Chemelectrochem 5 (2018) 1459–1466, https://doi.org/10.1002/celc.201800254.

[14] D.A. Agarkov, S.I. Bredikhin, S.V. Kiseleva, D.V. Matveev, A.V. Samoilov, A. B. Tarasenko, YuS. Fedotov, E.V. Tsipis, Solid oxide fuel cells' prospects for landfill gas utilization in Russia, Therm. Eng. 70 (2023) 73–79, https://doi.org/10.1134/S0040601523010019.

[15] E.V. Tsipis, V.V. Kharton, Electrode materials and reaction mechanisms in solid oxide fuel cells: a brief review. III. Recent trends and selected methodological aspects, J. Solid State Electrochem. 15 (2011) 1007–1040, https://doi.org/10.1007/s10008-011-1341-8.

[16] M. Pillai, Y. Lin, H. Zhu, R.J. Kee, S.A. Barnett, Stability and coking of direct-methane solid oxide fuel cells: effect of CO_2 and air additions, J. Power Sources 195 (2010) 271–279, https://doi.org/10.1016/j.jpowsour.2009.05.032.

[17] K.J. Yoon, S. Gopalan, U.B. Pal, Effect of Fuel Composition on performance of single-step cofired SOFCs, J. Electrochem. Soc. 154 (2007) B1080–B1087.

[18] E.L. Cussler, Diffusion: Mass Transfer in Fluid Systems, third ed., Cambridge University Press, Cambridge, 2009.

[19] M.W. Chase Jr., NIST-JANAF thermochemical tables, in: J. Phys. Chem. Ref. Data, fourth ed., American Chemical Society; New York, USA: American Institute of Physics for the National Institute of Standards and Technology, Washington, DC, USA, 1998. Monograph 9.

[20] Y. Matsuzaki, I. Yasuda, Electrochemical oxidation of H_2 and CO in a H_2 –H_2O –CO–CO_2 system at the interface of a Ni-YSZ cermet electrode and YSZ electrolyte, J. Electrochem. Soc. 147 (2000) 1630–1635, https://doi.org/10.1149/1.1393409.

[21] A.A. Khomenko, L.O. Apel'baum, F.S. Shub, S. Snagovsky, M.I. Temkin, Kinetics of the reaction of methane with water vapor and hydrogenation of carbon monoxide (reverse reaction) on the nickel surface, Kinet. Katal. 12 (1971) 423–429 (in Russian).

[22] P. Aguiar, C.S. Adjiman, N.P. Brandon, Anode-supported intermediate temperature direct internal reforming solid oxide fuel cell. I: model-based steady-state performance, J. Power Sources 138 (2004) 120–136, https://doi.org/10.1016/j.jpowsour.2004.06.040.

[23] Z. Jaworski, B. Zakrzewska, P. Pianko-Oprych, On thermodynamic equilibrium of carbon deposition from gaseous C-H-O mixtures: updating for nanotubes, Rev. Chem. Eng. 33 (2017) 217–235, https://doi.org/10.1515/revce-2016-0022.

[24] P. Aguiar, C.S. Adjiman, N.P. Brandon, Anode-supported intermediate-temperature direct internal reforming solid oxide fuel cell: II. Model-based dynamic performance and control, J. Power Sources 147 (2005) 136–147, https://doi.org/10.1016/j.jpowsour.2005.01.017.

[25] M. Fardadi, D.F. McLarty, F. Jabbari, Investigation of thermal control for different SOFC flow geometries, Appl. Energy 178 (2016) 43–55, https://doi.org/10.1016/j.apenergy.2016.06.015.